Case Studies in Chemical and Environmental Engineering 13 (2026) 101338

Contents lists available at ScienceDirect

Case Studies in Chemical and Environmental Engineering

journal homepage: www.sciencedirect.com/journal/case-studies-in-chemical-and-environmental-engineering

Case Report

Synergistic effects of combining ZIF-8 and graphene oxide inside cellulose acetate-based mixed matrix membranes on the removal of methylene blue

Putu Doddy Sutrisna [a,*], Pra Cipta Buana Wahyu Mustika [a], Candra Wijaya [a], Verdianto Indra Wijaya Sutama Putra [a], Putu Dhiyo Dharmayoga Denaswara [a], Ronaldo Pangestu Hadi [b], Aloisiyus Yuli Widianto [a], Edy Purwanto [a]

[a] Department of Chemical Engineering, University of Surabaya (UBAYA), Jl. Raya Kalirungkut (Tenggilis), Surabaya, 60293, Indonesia
[b] Department of Chemical and Biomolecular Engineering, Johns Hopkins University, 3400 N. Charles St., Baltimore, 21218, MD, USA

ARTICLE INFO

Keywords:
Mixed matrix membranes
Cellulose acetate
ZIF-8
Graphene oxide
Methylene blue

ABSTRACT

Mixed matrix membranes (MMMs) combining zeolitic imidazolate framework-8 (ZIF-8) and graphene oxide (GO) within a cellulose acetate (CA) matrix were fabricated via phase inversion for methylene blue (MB) dye removal. ZIF-8 introduced rigid microporous domains that enhanced dye retention through adsorption and steric hindrance, while GO improved membrane hydrophilicity and filler dispersion. SEM and XRD analyses confirmed uniform filler incorporation and partial structural ordering, whereas excessive GO loading reduced apparent crystallinity. ZIF-8 incorporation increased membrane hydrophobicity and reduced permeability; however, the addition of GO partially mitigated this effect, leading to improved flux relative to ZIF-8-only membranes while maintaining high rejection. The optimized CA/ZIF-8 + GO membrane achieved 99.7% MB removal, demonstrating a synergistic balance between permeability and selectivity. These findings highlight the potential of hybrid-filler CA-based MMMs as sustainable adsorptive ultrafiltration membranes for dye wastewater treatment, supporting SDG 6 and SDG 12.

1. Introduction

The rapid expansion of industrial activities, particularly in textile, paper, leather, and printing sectors, has resulted in the continuous release of dye-laden effluents into aquatic systems. Synthetic dyes, especially methylene blue (MB), are among the most common and persistent pollutants in wastewater. These compounds possess complex aromatic ring structures that are chemically stable and resistant to microbial degradation, leading to their accumulation in the environment [1,2]. The excessive presence of MB in water is not only toxic to aquatic organisms but also reduces light penetration, disrupting photosynthetic balance and overall ecosystem productivity [3]. Furthermore, long-term human exposure to such dyes can induce mutagenic and carcinogenic effects [4]. Therefore, developing efficient and sustainable approaches for dye removal and water purification is crucial to achieving the United Nations Sustainable Development Goals (SDG 6: Clean Water and Sanitation) and promoting responsible industrial wastewater management (SDG 12: Responsible Consumption and Production).

Conventional wastewater treatment technologies such as coagulation–flocculation, sedimentation, adsorption, and oxidative degradation have been widely employed for dye removal, yet each suffers from inherent limitations. Coagulation–flocculation and sedimentation are efficient primarily for suspended solids but are ineffective for dissolved organic dyes and require large treatment areas for continuous operation [5]. Simple filtration cannot efficiently separate dye molecules, as their molecular dimensions are much smaller than typical filter pore sizes [6]. Adsorption techniques using activated carbon or clay adsorbents can provide high initial removal efficiency but often face rapid saturation, regeneration difficulty, and secondary waste generation [7,8]. On the other hand, photocatalytic degradation and advanced oxidation processes offer high degradation efficiency but are limited by high energy demand, short catalyst lifetime, and poor scalability for industrial deployment [9,10]. Consequently, there is a growing demand for low-energy, high-selectivity, and re-useable membrane-based technologies capable of addressing complex dye wastewater streams.

Membrane separation has emerged as a powerful and energy-efficient alternative for wastewater treatment due to its low chemical

* Corresponding author.
E-mail address: pudod@staff.ubaya.ac.id (P.D. Sutrisna).

https://doi.org/10.1016/j.cscee.2026.101338
Received 20 October 2025; Received in revised form 15 January 2026; Accepted 31 January 2026
Available online 2 February 2026

input, scalability, and excellent selectivity [11]. Among different pressure-driven processes, microfiltration (MF), ultrafiltration (UF), nanofiltration (NF), and reverse osmosis (RO), UF and NF are particularly attractive for dye wastewater due to their ability to remove macromolecules and multivalent ions at moderate operating pressures. However, a long-standing challenge remains: the trade-off between permeability and selectivity, enhancing dye rejection typically results in reduced water flux [12,13]. Furthermore, polymeric membranes such as cellulose acetate (CA) or polyethersulfone (PES) are prone to fouling, pore blockage, and surface degradation, leading to diminished long-term stability [14,15].

To overcome these limitations, mixed matrix membranes (MMMs) have gained substantial attention as a new generation of functional membranes. MMMs incorporate nanostructured inorganic or hybrid fillers within a polymer matrix, combining the mechanical robustness and flexibility of polymers with the high porosity and tunable chemistry of the fillers [14,15]. Among various nanofillers, such as TiO_2, Fe_2O_3, SiO_2, carbon nanotubes (CNTs), and zeolites, the use of metal–organic frameworks (MOFs) has shown exceptional promise. MOFs are crystalline materials composed of metal ions and organic linkers, characterized by uniform pores, high surface area, and structural tunability. These features enable the design of membranes with selective adsorption, molecular sieving, and enhanced antifouling properties [16,17].

Within this family, zeolitic imidazolate frameworks (ZIFs) stand out for their zeolite-like topology and superior chemical and thermal stability. ZIF-8, formed by Zn^{2+} ions coordinated with 2-methylimidazolate linkers, exhibits microporous channels (3.4 Å), large surface area ($>1000\ m^2\ g^{-1}$), and resistance to water and mild alkaline conditions [18,19]. The positively charged imidazolate linkages allow electrostatic interaction with ionic dye molecules, while π–π stacking interactions between ZIF-8's aromatic rings and the aromatic structure of MB enhance adsorption and rejection [20]. Nevertheless, despite its excellent separation potential, the incorporation of ZIF-8 alone can increase membrane hydrophobicity, leading to reduced water permeability and greater fouling tendency [16].

To counter this, graphene oxide (GO) has emerged as a synergistic hydrophilic additive. GO contains abundant oxygenated functional groups that improve hydrophilicity, dispersibility, and interfacial compatibility with polymers [21]. When combined with ZIF-8, GO forms a dual-functional hybrid filler capable of enhancing both permeability and selectivity through complementary mechanisms. The lamellar structure of GO facilitates water transport pathways and prevents particle agglomeration, while ZIF-8 provides selective adsorption sites for dye molecules. Moreover, GO suppresses the hydrophobic effect of ZIF-8, resulting in improved water flux, antifouling performance, and dye rejection efficiency [10,18]. These synergistic properties have made ZIF-8/GO composites a promising direction for designing next-generation dye filtration membranes.

In this context, this study investigates a ternary mixed matrix membrane (MMM) system based on cellulose acetate (CA), ZIF-8, and graphene oxide (GO), fabricated using a scalable phase inversion process for dye wastewater treatment. In contrast to many ZIF-8/GO MMM studies that rely on petroleum-based polymers such as polyethersulfone or polyvinylidene fluoride, this work employs a biodegradable CA matrix, offering good chemical resistance, tunable porosity, and practical processability, making it suitable for environmentally oriented membrane applications [22]. Within the membrane structure, ZIF-8 acts as a microporous filler that enhances dye rejection through size exclusion and adsorption-related interactions, although excessive loading may reduce water permeability due to increased hydrophobicity and pore blockage. The incorporation of GO as a hydrophilic two-dimensional additive mitigates this limitation by improving polymer–filler compatibility, reducing ZIF-8 agglomeration, and facilitating water transport through the membrane. By systematically correlating membrane morphology, wettability, permeation flux, and dye rejection under identical fabrication conditions, this study demonstrates how the combined use of ZIF-8 and GO can balance permeability and selectivity, providing a practical and sustainable membrane design strategy for dye-contaminated wastewater treatment.

2. Materials and method

2.1. Materials

Cellulose acetate (CA) was procured from Sigma-Aldrich (USA). Acetone and formamide, also obtained from Sigma-Aldrich, were employed as solvents in the synthesis of CA-based membranes. For the preparation of ZIF-8 nanoparticles, zinc nitrate hexahydrate and 2-methylimidazole (Sigma-Aldrich) served as the metal precursor and organic linker, respectively, with methanol used as the solvent. Graphene oxide (GO) particles were likewise purchased from Sigma-Aldrich. Unless otherwise specified, all chemicals were of analytical grade and used without further purification.

2.2. Synthesis of ZIF-8 particles

The schematic representation of the ZIF-8 synthesis process is illustrated in Fig. 1a. Following the procedure reported in a previous study [23], ZIF-8 nanoparticles were synthesized by separately dissolving 3 g of zinc nitrate hexahydrate and 6.5 g of 2-methylimidazole in 200 mL of methanol. The two precursor solutions were subsequently mixed and stirred for 1.5 h to obtain a homogeneous mixture. The resulting suspension was centrifuged at 6800 rpm for 15–20 min to recover the ZIF-8 precipitate, which was then dried in an oven at 85 °C for 24 h. The dried ZIF-8 powder was later employed for the fabrication of mixed matrix membranes (MMMs). ZIF-8 and GO particles were characterized using SEM, XRD and BET. The morphology of particle was analyzed under Axia SEM. BET surface area of ZIF-8 was analyzed using nitrogen adsorption-desorption isotherms at 77K in a Micromeritic Tristar 3000 analyzer. XRD patterns of both particles were resulted from XRD analysis using Malvern Analytical X-ray diffraction.

2.3. Synthesis of cellulose acetate based MMMs

The schematic representation of the membrane fabrication process is illustrated in Fig. 1b. Following the procedure described by Ref. [24], mixed matrix membranes (MMMs) were prepared using a polymer solution composed of 20 wt% cellulose acetate (CA), 33 wt% formamide, and 47 wt% acetone, with 4 g of CA as the base polymer. ZIF-8 nanoparticles (5 and 10 wt% relative to CA) and graphene oxide (GO) particles (0.3, 0.6, and 1 wt% relative to CA) were incorporated in varying compositions. The mixture was magnetically stirred in a closed iodine flask for 24 h to achieve homogeneity, followed by degassing at room temperature for 24 h to eliminate trapped air bubbles. The resulting casting solution was then spread onto a glass plate using a stainless-steel casting knife and immediately immersed in a water coagulation bath for 10–20 min to induce phase inversion and membrane solidification. The membranes were subsequently stored in distilled water for 24 h prior to characterization.

The membrane morphology was examined using Axia scanning electron microscopy (SEM) by gold sputtering coating of sample before imaging, while the crystalline structure was analyzed by Malvern Analytical X-ray diffraction (XRD) and the chemical functionalities were identified through Shimadzu Tracer IR-100 Fourier-transform infrared spectroscopy (FTIR). The hydrophilicity of the membrane was analyzed using contact angle goniometer [DataPhysics Instruments, OCA25], which allowed for precise evaluation of wettability of the membranes.

2.4. Methylene blue filtration test

The schematic illustration of the methylene blue filtration test is presented in Fig. 1c–d. Methylene blue (MB) solutions were prepared by

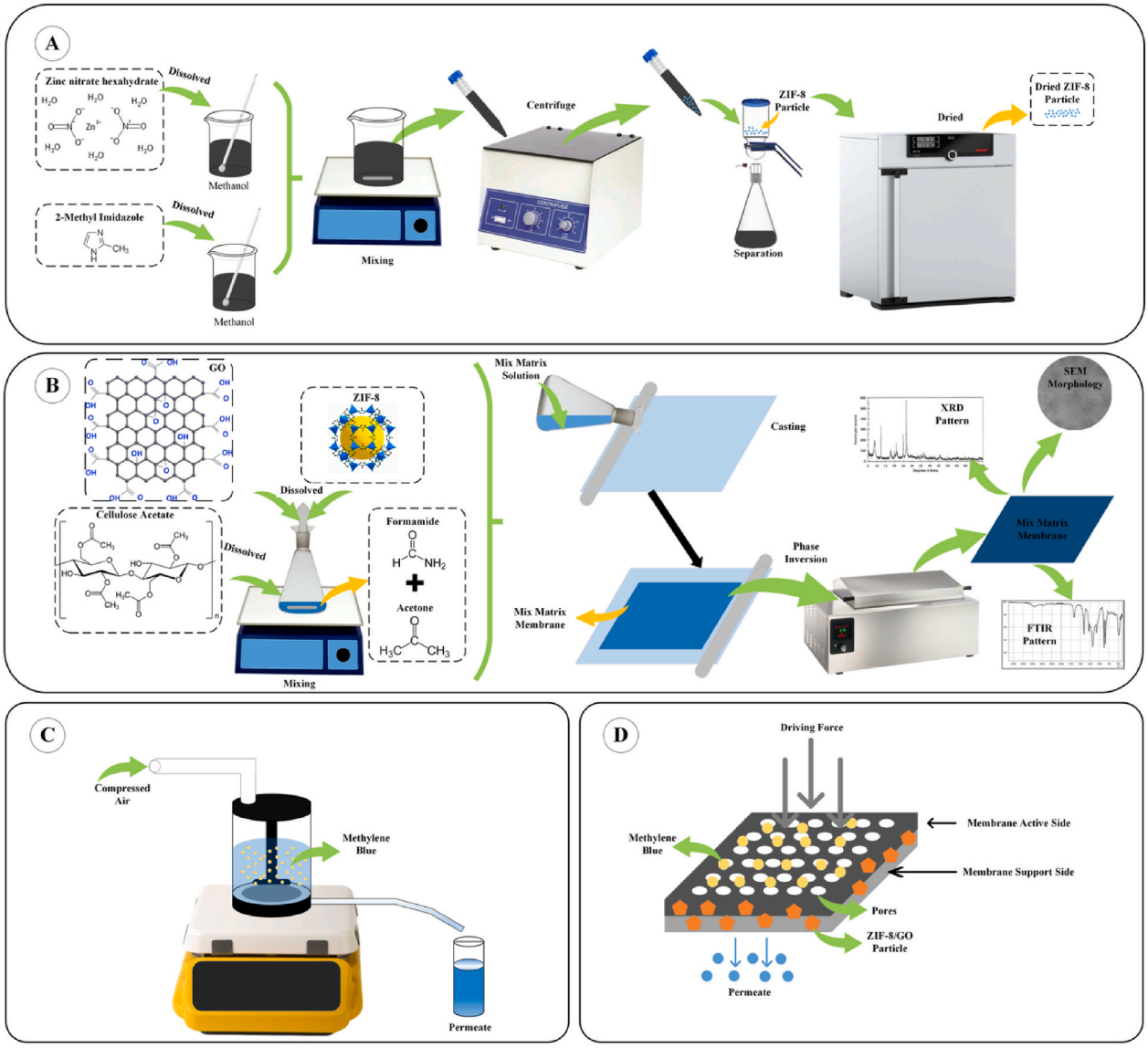

Fig. 1. Schematic diagram of (a) ZIF-8 synthesis, (b) membrane fabrication, and (c & d) filtration test.

dissolving 0.025 g and 0.05 g of MB powder in 500 mL of distilled water to obtain concentrations of 50 and 100 ppm, respectively. Circular membrane samples were mounted in a dead-end microfiltration cell. Prior to the filtration process, 150 mL of distilled water was passed through the membrane to ensure proper compaction and system pressurization. Subsequently, 150 mL of the prepared MB solution was introduced into the cell, and the permeate was collected until the entire feed had passed through the membrane.

The concentrations of MB in both the feed and permeate were analyzed using a UV–Vis spectrophotometer at a maximum absorption wavelength of 660 nm. The permeate flux (J) was determined according to Eq. (1).

$$J = V/A.t \tag{1}$$

where J (L m^{-2} h^{-1}) represents the permeate flux, V is the permeate volume (L), A is the effective membrane area (m^2), and t is the filtration time (h). The solute rejection (R) was calculated using Eq. (2).

$$R = \left(1 - C_p/C_f\right) \tag{2}$$

where C_p and C_f denote the solute concentrations in the permeate and feed, respectively.

Improved hydrophilicity-induced fouling resistance tendency studies involved three filtration cycles, each comprising a 30-min measurement of pure water flux (J_1), followed by a 30-min measurement of 100 ppm methylene blue solution, and another 30 min of pure water flux measurement after membrane cleaning (J_2). Flux recovery ratio (FRR) was then calculated according to Eq. (3)

$$\%\,FRR = \frac{J_2}{J_1} x100 \tag{3}$$

3. Results and discussions

3.1. Characterization of ZIF-8, GO, ZIF-8/CA, GO/CA, ZIF + GO/CA

For the synthesis of mixed matrix membranes, ZIF-8 and GO were employed as fillers inside the cellulose acetate matrix. ZIF-8 particles from room temperature synthesis had BET surface area of around 1639 m^2g^{-1} and several particles were found as agglomerates, as can be seen in SEM image of ZIF-8 in Fig. S2B, that should be treated carefully during the membrane synthesis by mixing the particles with polymer matrix

rigorously under high speed mixing. XRD analysis shows similar pattern with our previous publication (Fig. S2C) [23] indicating the formation of ZIF-8 particles. For GO particles, commercial GO used in this study also presented similar XRD patterns (Fig. S2D) with other studies on GO [25] and the SEM image in Fig. S2A also presents sheet of GO in agglomerates.

The functional group and crystallinity of the fabricated membranes are presented in Fig. 2, which compares pristine CA, CA/1% GO, CA/5–10% ZIF-8, and CA/5–10% ZIF-8 + 0.3–1% GO membranes. As shown in Fig. 2a, the FTIR spectrum of pristine CA exhibits characteristic peaks of O–H stretching vibrations at 3200–3500 cm^{-1}, C=O stretching at 1733 cm^{-1} corresponding to the ester groups in cellulose acetate, and C–O and C–O–C stretching bands in the 1030–1300 cm^{-1} region, attributed to ester functionalities and ether linkages along the cellulose backbone [26]. For the CA/GO membrane, the FTIR spectra display similar absorption bands to those of pristine CA, with no appearance of new peaks, indicating chemical compatibility between GO and the CA matrix. The characteristic bands of GO, including O–H (3300–3500 cm^{-1}), C=O (≈1750 cm^{-1}), C–O–C (1230–1340 cm^{-1}), and C–O (1042 cm^{-1}), overlap with those of CA [27,28]. The coincidence of these functional groups suggests strong interfacial interactions, likely hydrogen bonding and other intermolecular forces, promoting uniform GO dispersion within the CA matrix [29]. Similarly, the FTIR spectra of ZIF-8 particles is shown in Fig. S1. The FTIR spectrum of synthesized ZIF-8 features distinct peaks at 1146 cm^{-1} (aromatic C–N stretching), 1400–1450 cm^{-1} (aromatic C=C stretching), and 1570 cm^{-1} (C=N stretching) [30,31], however, these signals are largely masked by the dominant O–H and C=O vibrations of the CA matrix, consistent with earlier reports [32]. Furthermore, the incorporation of both GO and ZIF-8 fillers at various loadings (CA/ZIF-8 + GO) produces only minor shifts or negligible changes in the FTIR spectra, confirming the absence of new chemical bonds and the physical blending nature of the mixed matrix system.

The crystallinity feature of the resulted membranes was determined by XRD analysis as shown in Fig. 2b, which in this case is the cellulose acetate membranes with ZIF-8 and/or GO filler. According to several studies, cellulose acetate membranes have amorphous peaks at positions 5-15°, 15-25°, and 35-50° [24], ZIF-8 has several main peaks at position 7.30°; 10.35°; 12.70°; 14.80°; 16.40°; and 18° [10], while GO only had one peak at 10.30° [28]. In the composite membranes, several crystalline peaks appear within 5°–20°, primarily corresponding to ZIF-8 diffraction. A broad hump at 20°–25° likely originates from the semi-crystalline domains of CA, while the weak signals observed at 40°–45° can be assigned to amorphous polymeric regions [33,34]. The slightly increased peak intensity around 20°–25° is consistent with the incorporation of ZIF-8, suggesting partial structural ordering due to filler–matrix interactions [32,35]. Interestingly, in the membrane containing 10% ZIF-8, no distinct diffraction peaks were observed between 10° and 20° (2θ). This could be attributed to the uneven dispersion or possible agglomeration of ZIF-8 particles within the CA matrix, resulting in localized regions with reduced crystalline content [36,37]. According to previous study [38], the addition of GO up to an optimal concentration can enhance the apparent crystallinity or peak sharpness of a polymer composite, however, beyond this threshold, further GO loading diminishes crystallinity due to the amorphous and defect-rich structure of GO [11]. A similar trend was observed in this study, where increasing GO loading enhanced the peak intensity, but a further increase led to decreased crystallinity [28]. This reduction may be explained by the dominance of GO's disordered structure, which disrupts the polymer chain arrangement and reduces overall crystallinity [28,29].

The surface morphology of the synthesized MMMs observed by SEM at 10,000 × magnification is shown in Fig. 3(a–j). The pristine CA membrane (Fig. 3a) displayed a smooth and homogeneous surface with the largest pore diameter 0.5-1 μm, typical of a compact and continuous polymer film formed through solvent evaporation in the absence of inorganic fillers. The incorporation of 1% GO (Fig. 3b) produced a still smooth and relatively homogeneous surface but with noticeably smaller pore sizes. This reduction in pore size is attributed to the planar GO nanosheets restricting polymer chain mobility during phase inversion, resulting in a tighter packing structure [39]. In addition, the presence of oxygen-containing functional groups on GO enables hydrogen bonding with CA, improving interfacial compatibility and maintaining surface uniformity [29]. With the addition of 5% ZIF-8 (Fig. 3c), the surface remained smooth and homogeneous, yet the pores appeared smaller than those in pristine CA and GO-modified membranes. This can be explained by the fine dispersion of ZIF-8 particles within the polymer matrix, which occupy free volume and act as nucleation centers, thereby refining the pore structure [40]. When GO was co-introduced with 5% ZIF-8 (Fig. 3d–f), the surface gradually became rougher with increasing GO content. The appearance of uneven texture and visible agglomerates at higher GO loadings suggests that excessive GO promotes π–π stacking and filler–filler interactions, leading to particle clustering and reduced homogeneity [28,38,41]. These agglomerations also cause local stress variations during film formation, contributing to the rougher topography. A similar pattern was observed for membranes containing 10% ZIF-8 (Fig. 3g–j). Increasing the ZIF-8 content from 5% to 10% resulted in a noticeably rougher surface and visible agglomerates, indicating that excessive inorganic filler loading surpasses the polymer's ability to maintain uniform dispersion. The introduction of GO into the 10% ZIF-8 system (Fig. 3h–j) further intensified surface roughness, with clear aggregation at 0.6% GO and severe agglomeration at 1% GO. The rough surface morphology at high filler concentrations likely arises from limited interfacial bonding and filler–filler association, as both ZIF-8 and

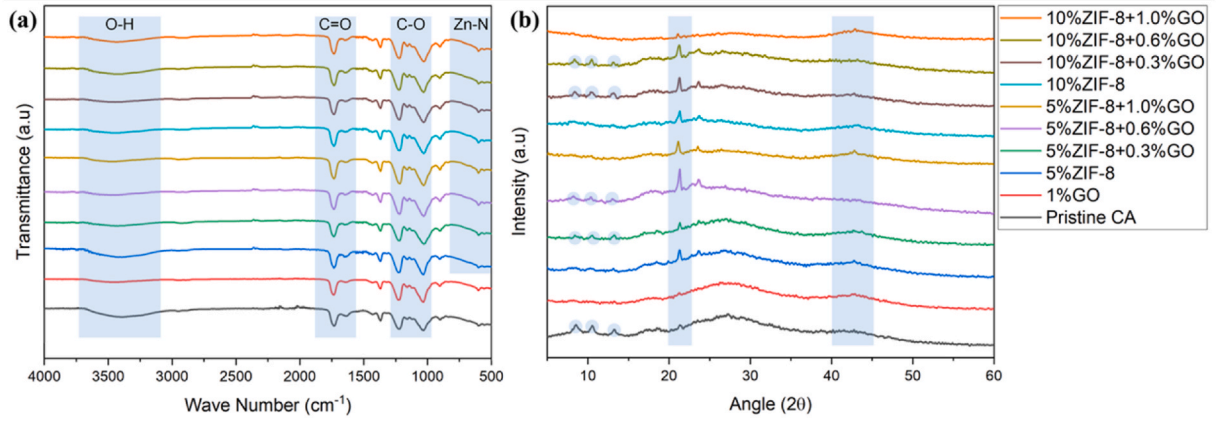

Fig. 2. (a) FTIR spectra and (b) XRD patterns of various membranes.

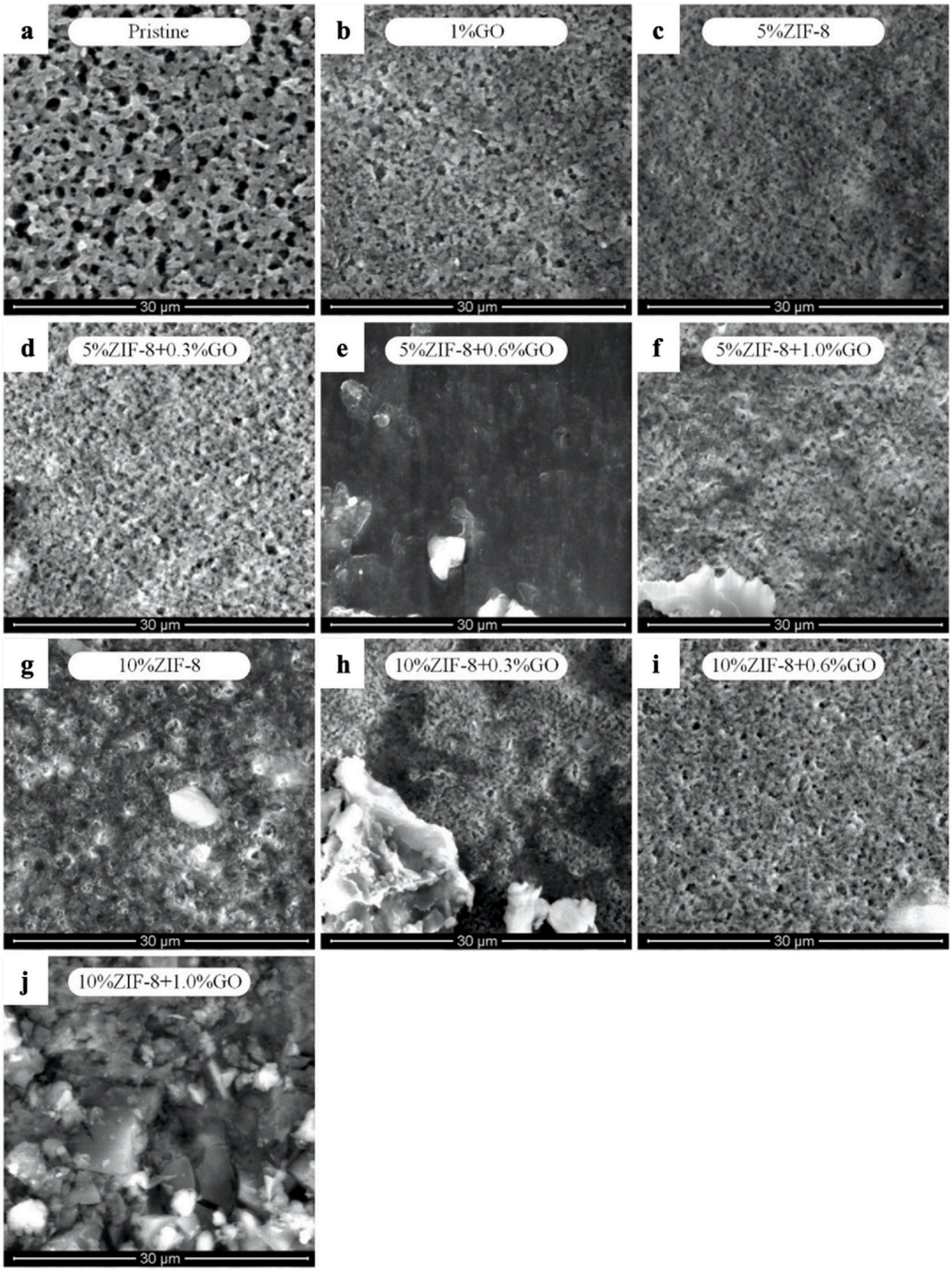

Fig. 3. SEM analysis result by 10000× magnification on (a) pristine CA, (b) CA/1% GO, (c) CA/5% ZIF-8, (d) CA/5% ZIF-8+0.3% GO, (e) CA/5% ZIF-8+0.6% GO, (f) CA/5% ZIF-8+1% GO, (g) CA/10% ZIF-8, (h) CA/10% ZIF-8+0.3% GO, (i) CA/10% ZIF-8+0.6% GO, (j) CA/10% ZIF-8+1% GO.

GO possess high surface energies that favor aggregation when not adequately stabilized by the polymer matrix [29,42]. In conclusion, the SEM results reveal that increasing ZIF-8 and GO loadings lead to a progressive transition from smooth and homogeneous to rough and agglomerated surfaces, while simultaneously reducing pore size at moderate concentrations. This morphological evolution reflects the balance between enhanced filler–polymer interactions at low to moderate loadings and aggregation-dominated behavior at higher loadings. Consequently, moderate filler compositions ($\leq$5% ZIF-8 and $\leq$0.6% GO) are favorable for achieving uniform dispersion and controlled pore formation, whereas higher filler ratios induce aggregation and surface roughness that may compromise mechanical and separation performance [42].

The surface wettability of the membranes was examined as shown in Fig. S3. The 10% ZIF-8 membrane exhibited the highest contact angle of around 86.5^{o} compared to 76.98^{o} of pure CA membrane, indicating the most hydrophobic surface among the tested samples. This behavior is consistent with previous studies reporting that ZIF-8 incorporation tends to reduce membrane surface hydrophilicity because the imidazolate linkers are relatively hydrophobic and limit hydrogen bonding with water molecules. In addition, excessive ZIF-8 loading may reduce surface porosity and expose fewer polar groups on the membrane surface

[43]. When 1% GO was co-incorporated with ZIF-8 (10 % ZIF-8/1 % GO), the contact angle decreased significantly to 73.8°, suggesting improved surface hydrophilicity. This can be attributed to the abundant oxygen-containing functional groups (–OH, –COOH, –C=O) on GO that can form hydrogen bonds with water, enhancing the membrane–water interaction. The presence of GO also improves filler–polymer interfacial compatibility, leading to a more homogeneous surface that facilitates water spreading across the membrane [10]. The 1% GO membrane showed the lowest contact angle of around 57.95°, confirming the highest hydrophilicity. The dominant influence of GO's polar functional groups over the cellulose acetate matrix significantly increases surface energy and water affinity, consistent with other reports that GO addition markedly enhances membrane wettability and antifouling performance [29]. Therefore, the observed trend in wettability test (10% ZIF-8 > 10% ZIF-8/1% GO > 1% GO) aligns with the synergistic effects of ZIF-8 and GO reported in MMMs systems [44]. The introduction of GO counterbalances the hydrophobic nature of ZIF-8, resulting in improved hydrophilicity and potential enhancement in water flux.

3.2. MMMs performance test on methylene blue filtration

The separation performance of the fabricated mixed matrix membranes (MMMs) was evaluated through methylene blue (MB) filtration tests, with permeate flux and rejection efficiency serving as the primary performance indicators, representing membrane permeability and selectivity, respectively. Permeate flux, defined as the volume of water passing through the membrane per unit area and time under a given pressure, reflects the membrane's water transport capability, whereas rejection efficiency describes the reduction in MB concentration between the feed and permeate, indicating dye removal effectiveness. Based on the observed surface pore morphology (0.5–1 μm) and consistently high MB rejection, the membranes are classified as adsorptive ultrafiltration membranes. In this system, dye separation is governed mainly by adsorption, pore blockage, and cake-enhanced retention mechanisms, while water permeation is primarily controlled by membrane hydrophilicity and pore connectivity.

Fig. 4 illustrates the variation of permeate flux over filtration time for MB solutions at concentrations of (a) 50 ppm and (b) 100 ppm, using pristine CA and MMMs incorporated with different loadings of ZIF-8 and GO. In both conditions, the flux of all membranes declined gradually with time, which can be attributed to the progressive accumulation of dye molecules on the membrane surface and within the pores, leading to concentration polarization and fouling layer formation [37,45]. The pristine CA membrane exhibited the highest flux values, ranging from 70.38 to 68.85 L m^{-2} h^{-1} at 50 ppm and 57.69 to 56.15 L m^{-2} h^{-1} at 100 ppm. In contrast, MMMs containing 5% ZIF-8 showed lower fluxes in the ranges of 37.72–32.33 L m^{-2} h^{-1} (50 ppm) and 36.95–30.41 L m^{-2} h^{-1} (100 ppm). Further increasing the ZIF-8 content to 10% reduced the flux even more, to 24.63–22.71 L m^{-2} h^{-1} (50 ppm) and 23.09–19.25 L m^{-2} h^{-1} (100 ppm). The decline in flux with increasing ZIF-8 loading can be attributed to the partial hydrophobicity of ZIF-8 particles, which hinders water transport through the membrane pores and increases hydraulic resistance [35,46]. Higher ZIF-8 contents can also promote rigidification and swelling of the polymer matrix, further limiting pore connectivity and effective water passage [42]. Conversely, the incorporation of GO into the MMMs improved water flux compared to the ZIF-8-only membranes. As shown in Fig. 4, flux values increased with higher GO loading (0.3–1%) for both 5% and 10% ZIF-8 membranes, confirming that the hydrophilic oxygenated functional groups (–OH, –COOH, –C=O) on GO enhanced water–membrane interactions and facilitated faster permeation [47]. Among all MMM configurations, the CA/1% GO membrane demonstrated the highest initial flux, reaching 68.91 L m^{-2} h^{-1} at 50 ppm and 83.92 L m^{-2} h^{-1} at 100 ppm. Nevertheless, in the absence of ZIF-8, a rapid decline in flux was observed during filtration, indicating faster fouling and weaker structural stability compared to hybrid ZIF-8/GO membranes. This finding highlights the complementary roles of GO in enhancing hydrophilicity and ZIF-8 in maintaining structural integrity and improved hydrophilicity-induced fouling resistance tendency within the mixed matrix system [35,42]. As shown in Fig. S4, an increase in feed concentration from 50 ppm to 100 ppm consistently resulted in lower flux values for all MMMs. The higher dye concentration increased the adsorption of MB molecules on the membrane surface, thereby forming a thicker boundary layer that obstructed water permeation [48]. Overall, these flux behaviors are in good agreement with the SEM, XRD, and wettability results. SEM images revealed that higher ZIF-8 loadings produced denser and less porous morphologies, while XRD analysis confirmed increased crystallinity with ZIF-8 incorporation. Meanwhile, GO addition improved surface wettability, as indicated by lower contact angle values, demonstrating its compensating effect on the hydrophobicity of ZIF-8 and its contribution to the enhanced water flux observed in the MMMs.

As shown in Fig. 5, all membranes demonstrated high rejection efficiencies (>88%) toward MB, confirming their excellent separation performance under ultrafiltration conditions. The pristine CA membrane showed the lowest rejection (93.6% at 50 ppm and 92.4% at 100 ppm), consistent with its smooth and homogeneous surface morphology with larger pores (0.5–1 μm) observed in Fig. 3a. The relatively open structure of pristine CA allows limited passage of MB molecules primarily through steric pathways. Incorporating 1% GO significantly improved rejection to 98.9% at 50 ppm, although a decline to 88.7% at 100 ppm occurred. The improvement at lower concentration is attributed to pore size reduction and tighter structure formation, as shown in Fig. 3b, where GO particles restrict polymer chain mobility during phase

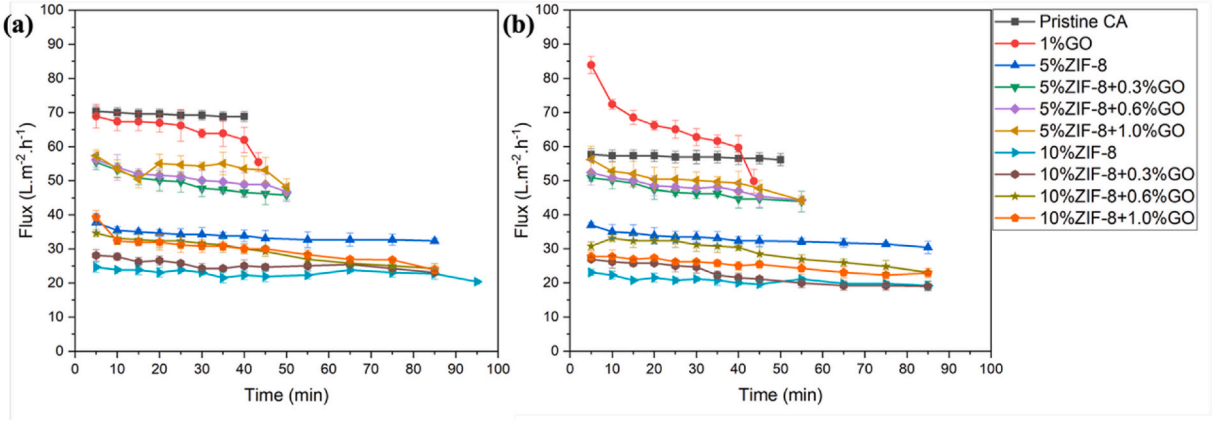

Fig. 4. Time-dependent flux profiles of MMMs with different filler compositions at MB concentrations of (a) 50 ppm and (b) 100 ppm.

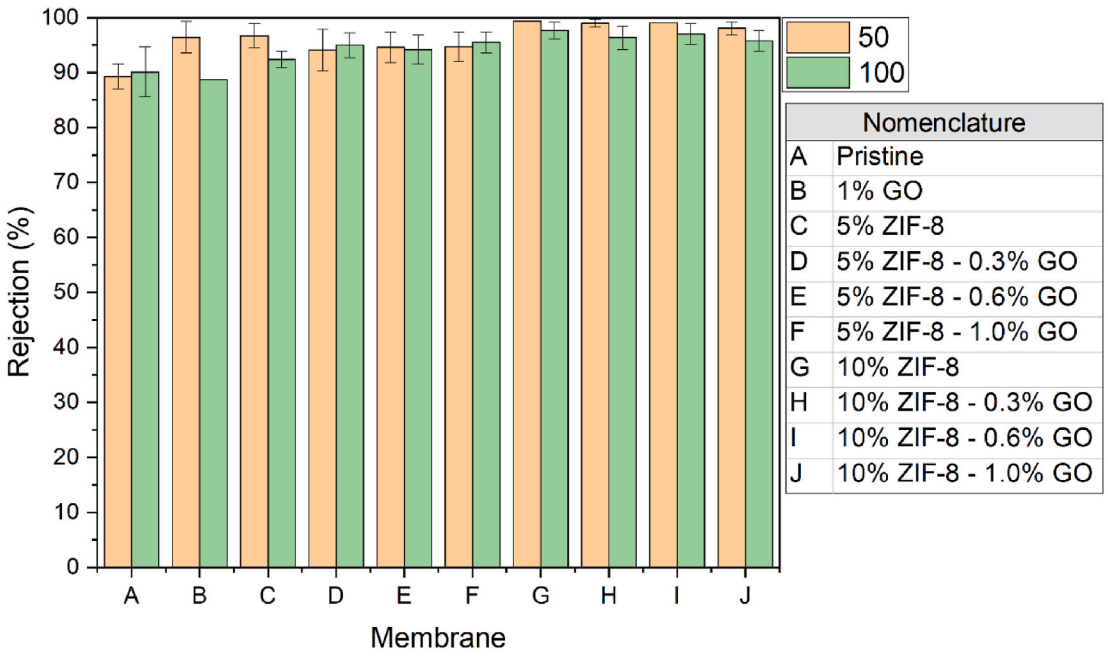

Fig. 5. MB rejection performance of membrane containing different filler compositions.

inversion. Furthermore, the oxygenated functional groups (–OH, –COOH, –C=O) on GO introduce weak negative surface charge, enhancing electrostatic repulsion toward the cationic MB molecules. The reduced performance at higher concentration likely arises from adsorption saturation and concentration polarization, which partially suppress the repulsion effect [25,49]. For ZIF-8-modified membranes, both 5% and 10% loadings enhanced dye rejection compared to pristine CA, achieving 98.9% and 94.0% for the 5% ZIF-8 membrane and 99.6% and 98.7% for the 10% ZIF-8 membrane at 50 and 100 ppm, respectively. The XRD patterns (Fig. 2b) confirm crystalline ZIF-8 domains between 5° and 20°, indicating the formation of microporous frameworks that narrow the effective pore size and create tortuous diffusion pathways, enhancing steric hindrance against dye transport [50]. However, SEM images (Fig. 3g) reveal that at higher ZIF-8 loadings (10%), surface roughness and agglomeration become more evident, which may slightly compromise homogeneity despite improved selectivity. When GO and ZIF-8 were co-incorporated, the hybrid membranes exhibited the most consistent and highest rejection values, ranging from 97.4 to 99.7% at 50 ppm and 97.7–98.7% at 100 ppm. This performance enhancement reflects synergistic structural and interfacial effects: ZIF-8 contributes rigidity and fine micropores, while GO promotes uniform filler dispersion and reinforces polymer–filler interactions. SEM observations (Fig. 3d–f, h–j) show smooth and uniform surfaces at moderate loadings (≤5% ZIF-8 and ≤0.6% GO), whereas excessive filler concentrations induce aggregation and roughness. The wettability test data (Fig. S3) further correlate with rejection performance. The 10% ZIF-8 membrane showed the highest contact angle (most hydrophobic), while the addition of GO reduced the contact angle significantly, improving hydrophilicity and thus facilitating water permeability and improved hydrophilicity-induced fouling resistance tendency. The enhanced hydrophilicity also supports a more stable electrostatic double layer on the membrane surface, which contributes to electrostatic repulsion against MB during filtration [25]. Across both dye concentrations, the rejection remained nearly constant for all hybrid membranes, indicating that size exclusion is the dominant mechanism, with electrostatic repulsion playing a reinforcing role, especially for GO-containing compositions. The high and stable rejection confirms strong membrane integrity and compatibility between polymer and fillers, without evidence of defect-induced leakage or filler leaching. In conclusion, the superior rejection of the GO/ZIF-8 hybrid ultrafiltration membranes arises from the combined steric and electrostatic mechanisms, supported by structural evidence from XRD, SEM, and wettability analyses. ZIF-8 provides microporous rigidity and tortuous pathways, while GO enhances hydrophilicity, introduces mild surface charge, and improves filler dispersion. Moderate filler ratios (≤5% ZIF-8 and ≤0.6% GO) yield a compact, uniform structure with optimal balance between hydrophilicity and selectivity, resulting in nearly complete MB rejection and strong potential for dye wastewater treatment applications.

The comparison between flux and rejection during MB filtration shows that the 10% ZIF-8 membrane achieved the highest rejection (99.6% and 98.7%) but suffered from low flux due to its dense and hydrophobic structure. The addition of 0.6% GO effectively improved flux while maintaining similar rejection (99.7% and 98.6%), demonstrating that moderate GO loading enhances water–membrane interaction and reduces dye accumulation without compromising selectivity. A comparable trend was observed in the 5% ZIF-8 series, where GO addition maintained high MB rejection while markedly increasing flux. These results indicate that ZIF-8 primarily controls selectivity through its microporous framework, while GO improves hydrophilicity and electrostatic repulsion toward MB, resulting in a synergistic balance between permeability and selectivity in the mixed matrix membranes.

Further test on flux recovery ratio (FRR) showed that the introduction of GO improved the percentage of FRR of the membrane as can be seen in Fig. S5. Compared to pristine CA, the presence of GO improved the hydrophilicity of the membrane and improved the fouling resistance tendency of the membrane. The presence of ZIF-8 and GO inside CA matrix also improved fouling resistance tendency as the percentage of FRR of ZIF-8/GO-based membrane was higher than its pure CA membrane counterpart.

3.3. MMMs performance improvement mechanisms and comparison with previous studies

Fig. 6 illustrates the proposed separation mechanism of methylene blue (MB) by the CA/ZIF-8 + GO mixed matrix membranes. The incorporation of ZIF-8 nanoparticles into the cellulose acetate (CA) matrix significantly enhances dye rejection compared to pristine CA membranes. This enhancement is primarily attributed to steric

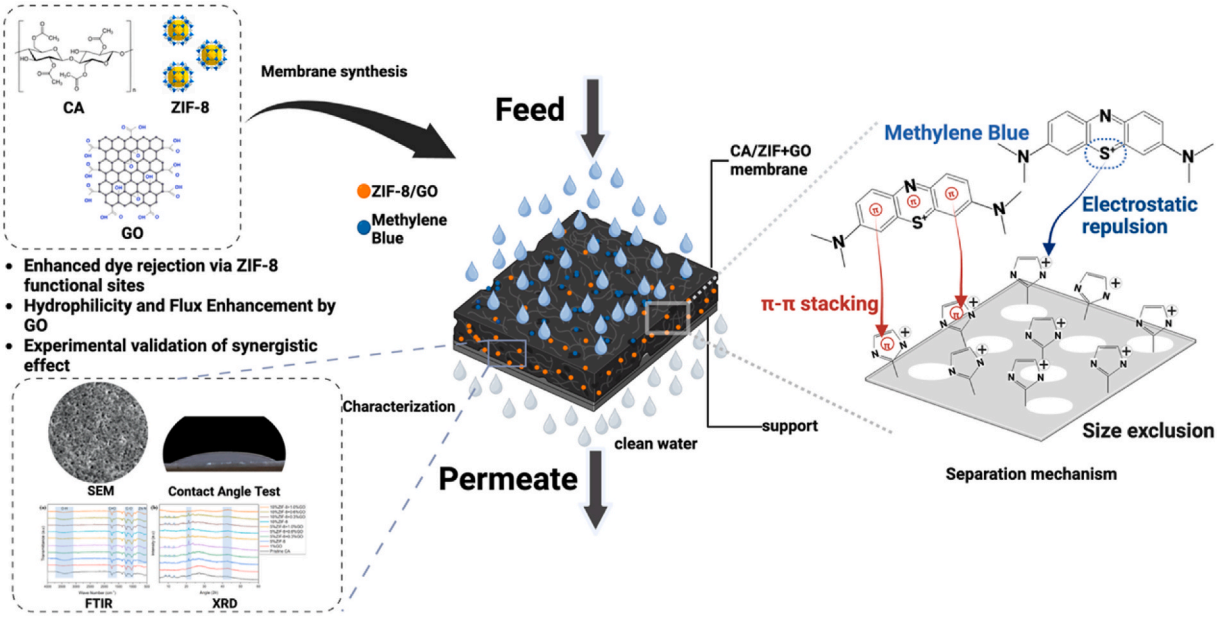

Fig. 6. Separation mechanism of MB by CA/ZIF-8 + GO MMMs.

hindrance, adsorption, and tortuous transport pathways introduced by the rigid ZIF-8 framework. The aromatic imidazolate linkers of ZIF-8 enable π–π stacking interactions with the aromatic rings of MB, promoting dye adsorption and retarding solute transport through the membrane structure [18].

It should be noted that methylene blue is a cationic dye; therefore, direct electrostatic attraction between ZIF-8 and MB is not expected. Instead, electrostatic interactions play a secondary role and are mainly associated with graphene oxide (GO), which introduces oxygen-containing functional groups that impart mild negative surface charge to the membrane. This negative surface charge enhances electrostatic repulsion toward cationic MB molecules, reinforcing dye retention. Meanwhile, GO improves membrane hydrophilicity and facilitates water transport via hydrogen bonding, partially compensating for the permeability reduction caused by ZIF-8 incorporation. The combined effects of adsorption, steric hindrance, π–π interactions, and enhanced hydrophilicity result in a synergistic balance between permeability and selectivity in the hybrid CA/ZIF-8 + GO membranes [25,38].

The performance of synthesized CA/ZIF-8+GO from this study also compared with other MMMs studies (CA and PES matrices) as summarized in Table 1. Incorporating functional fillers such as ZIF-8, MIL-53(Fe), GO, or PRS significantly improves dye rejection compared to pristine polymer membranes. For example, CA with 0.25% ZIF-8 achieved 85 % removal of crystal violet due to electrostatic attraction and π–π stacking between dye molecules and the imidazolate rings of ZIF-8 [32]. Similarly, PES with 0.5% ZIF-8 reached 95.4 % rejection for Congo Red [53], while CA with 0.75% MIL-53(Fe) exhibited 98 % rejection of Direct Yellow [52]. The use of 2% GO in CA enhanced hydrophilicity and achieved 97 % Safranin-O rejection [5], whereas PES with PRS achieved 99.8 % Congo Red rejection [51], emphasizing the diverse mechanisms, electrostatic interaction, hydrogen bonding, and adsorption, that govern dye separation. In comparison, the present study achieved the highest performance with 99.7 % methylene blue removal using a dual-filler system of 10% ZIF-8 + 0.6% GO in a CA matrix. The synergistic effect of ZIF-8 and GO overcomes the conventional trade-off between flux and rejection observed in single-filler membranes. ZIF-8 provides abundant adsorption sites and positive surface charge for electrostatic attraction with the cationic component of methylene blue, while GO introduces hydrophilic oxygenated groups that facilitate water transport. Consequently, the CA/ZIF-8/GO MMM demonstrates superior selectivity, and permeability, offering a highly efficient strategy for dye wastewater purification.

Table 1
Comparison of this study with recently published MMMs literatures.

Polymer Matrix	Filler	Membrane fabrication	Dye Wastewater Type	Dye rejection	References
CA	0.25% ZIF-8	Phase inversion	Crystal Violet	85%	[32]
PES	66.4 mg PRS	One-step NIPS	Congo Red	99.8%	[51]
CA	0.75% MIL-53 (Fe)	Phase inversion	Direct Yellow	98%	[52]
PES	0.5% ZIF-8	NIPS	Congo Red	95.4%	[53]
CA	2% GO	Phase inversion	Safranin-O	97%	[28]
CA	10% ZIF-8+0.6% GO	Phase inversion	Methylene Blue	99.7%	This study

CA: cellulose acetate; PES: polyethersulfone; PRS: propolis; GO: graphene oxide; NIPS: non-solvent induced phase separation.

4. Conclusion

Cellulose acetate-based mixed matrix membranes (MMMs) incorporating ZIF-8 and GO were successfully synthesized and evaluated for methylene blue removal from aqueous solutions. Structural analyses confirmed the physical integration of both fillers within the CA matrix without new chemical bonding, while morphological observations revealed a transition from smooth to rough surfaces with increasing filler content. ZIF-8 enhanced dye rejection through electrostatic and π–π interactions but reduced permeability due to its hydrophobic nature and pore-blocking effect. In contrast, GO improved hydrophilicity and created additional water-transport pathways. The optimal composition, 10 wt% ZIF-8 + 0.6 wt% GO, achieved the highest overall performance, combining high rejection (99.7 %) with increased flux relative to ZIF-8-only membranes. This synergistic configuration effectively mitigates the flux–rejection trade-off, demonstrating that hybrid fillers can be tuned to balance selectivity, permeability, and improved hydrophilicity-

induced fouling resistance tendency. The findings highlight the potential of CA/ZIF-8 + GO MMMs as scalable and environmentally friendly membranes for industrial dye wastewater purification and other advanced separation processes.

CRediT authorship contribution statement

Putu Doddy Sutrisna: Writing – original draft, Supervision, Methodology, Funding acquisition, Conceptualization. **Pra Cipta Buana Wahyu Mustika:** Writing – review & editing, Validation, Formal analysis. **Candra Wijaya:** Writing – review & editing, Visualization. **Verdianto Indra Wijaya Sutama Putra:** Visualization, Investigation, Data curation. **Putu Dhiyo Dharmayoga Denaswara:** Investigation, Formal analysis, Data curation. **Ronaldo Pangestu Hadi:** Writing – review & editing, Validation. **Aloisiyus Yuli Widianto:** Writing – review & editing, Validation. **Edy Purwanto:** Writing – review & editing, Validation.

Declaration of competing interest

The authors declare that they have no known competing financial interests or personal relationships that could have appeared to influence the work reported in this paper.

Acknowledgments

The authors gratefully acknowledge the financial support from Ministry of Research, Technology and Higher Education of Indonesia under National Competitive Fundamental Research Grant (contract number 017/SP-Lit/LPPM-01/Diktisaintek/FT/VI/2025).

Appendix A. Supplementary data

Supplementary data to this article can be found online at https://doi.org/10.1016/j.cscee.2026.101338.

Data availability

Data will be made available on request.

References

[1] C. Hou, B. Hu, J. Zhu, Photocatalytic Degradation of Methylene Blue over TiO2 Pretreated with Varying Concentrations of Naoh, 8, 2018, p. 575, https://doi.org/10.3390/CATAL8120575.

[2] H. Fansuri, M.N. Alief, N. Nurlina, S.D. Nurherdiana, MohdM. Al Bakri Abdullah, S. Subaer, Photocatalytic geopolymer membranes from Indonesian fly ash: TiO2 integration, stability, and methylene blue degradation, Case Stud. Chem. Environ. Eng. 12 (2025) 101292, https://doi.org/10.1016/J.CSCEE.2025.101292.

[3] P. Prasetya, A. Awaluddin, M. Muhdarina, E. Saputra, N.N. Linggawati A, Solvothermal synthesis of α-MnO2 and Mn2O3 for efficient catalytic dye degradation, Case Stud. Chem. Environ. Eng. 12 (2025) 101242, https://doi.org/10.1016/J.CSCEE.2025.101242.

[4] M. Abril-González, D. Seminario, V. Pinos-Vélez, E.-P.P. Vele A, An activated steel scale waste catalyst to degrade Methylene Blue via the Heterogeneous Fenton Process, Case Stud. Chem. Environ. Eng. 10 (2024) 100857, https://doi.org/10.1016/J.CSCEE.2024.100857.

[5] I.M.J. Iloamaeke, S.I. Atune, U.C. Onyeije, T.U. Onuegbu, Optimization of coagulation-flocculation process for colour removal in purification of paint industry effluent using novel seed of Spondias mombin Linn, Desalination Water Treat. 323 (2025) 101284, https://doi.org/10.1016/J.DWT.2025.101284.

[6] J. Han, P. Wu, J. Peng, S. Xia, X. Liu, Ultrafast and efficient selective separation of low-molecular-weight dyes via an advanced adsorptive membrane, Colloids Surf. A Physicochem. Eng. Asp. 726 (2025) 138005, https://doi.org/10.1016/J.COLSURFA.2025.138005.

[7] W. Wiśniewska, P. Nowicki, J. Bujdák, Controversial issues related to dye adsorption on clay minerals, Crit. Rev. 28 (2023) 6951, https://doi.org/10.3390/MOLECULES28196951.

[8] N.R.J. Hynes, J.S. Kumar, H. Kamyab, J.A.J. Sujana, O.A. Al-Khashman, , et al. Y. Kuslu, Modern enabling techniques and adsorbents based dye removal with sustainability concerns in textile industrial sector -A comprehensive review, J. Clean. Prod. 272 (2020) 122636, https://doi.org/10.1016/J.JCLEPRO.2020.122636.

[9] D. Blažeka, J. Car, N. Klobučar, A. Jurov, J. Zavašnik, A. Jagodar, Photodegradation of methylene blue and rhodamine B using laser-synthesized ZnO nanoparticles, Materials 13 (2020) 4357, https://doi.org/10.3390/MA13194357, 2020;13:4357, 13 (2020) 4357.

[10] N. Ahmad, A. Samavati, N.A.H.M. Nordin, J. Jaafar, A.F. Ismail, N.A.N.N. Malek, Enhanced performance and antibacterial properties of amine-functionalized ZIF-8-decorated GO for ultrafiltration membrane, Separ. Purif. Technol. 239 (2020) 116554, https://doi.org/10.1016/j.seppur.2020.116554.

[11] K. Zuo, K. Wang, R.M. DuChanois, Q. Fang, E.M. Deemer, X. Huang, R. Xin, I. A. Said, Z. He, Y. Feng, W. Shane Walker, J. Lou, M. Elimelech, X. Huang, Q. Li, Selective membranes in water and wastewater treatment: role of advanced materials, Mater. Today 50 (2021) 516–532, https://doi.org/10.1016/j.mattod.2021.06.013.

[12] K. Tao, Y. Zhang, Y. Song, Z. Chen, Y. Wang, Y. Wang, PEI-SiO2/GO nanofiltration membrane: achieved high water permeability and dye rejection rate, J. Environ. Chem. Eng. 13 (2025) 115011, https://doi.org/10.1016/J.JECE.2024.115011.

[13] I.A. Khan, K.M. Deen, E. Asselin, M. Yasir, R. Sadiq, N.M. Ahmad, Boosting water flux and dye removal: advanced composite membranes incorporating functionalized AC-PAA for wastewater treatment, J. Ind. Eng. Chem. 145 (2025) 705–720, https://doi.org/10.1016/J.JIEC.2024.10.067.

[14] Y. Cheng, Y. Ying, S. Japip, S.D. Jiang, T.S. Chung, S. Zhang, Advanced porous materials in mixed matrix membranes, Adv. Mater. 30 (2018) 1802401, https://doi.org/10.1002/ADMA.201802401, 30 (2018) 1802401.

[15] R.P. Pandey, P.A. Rasheed, T. Gomez, R.S. Azam, K.A. Mahmoud, A fouling-resistant mixed-matrix nanofiltration membrane based on covalently cross-linked Ti3C2TX (MXene)/cellulose acetate, J. Membr. Sci. 607 (2020) 118139, https://doi.org/10.1016/J.MEMSCI.2020.118139.

[16] Y. Li, Z. Lin, X. Wang, Z. Duan, P. Lu, S. Li, High-hydrophobic ZIF-8@PLA composite aerogel and application for oil-water separation, Sep. Purif. Technol. 270 (2021) 118794, https://doi.org/10.1016/J.SEPPUR.2021.118794.

[17] S. Zhou, O. Shekhah, J. Jia, J. Czaban-Jóźwiak, P.M. Bhatt, A. Ramírez, et al., Electrochemical synthesis of continuous metal–organic framework membranes for separation of hydrocarbons, Nat. Energy 6 (2021) 882–891, https://doi.org/10.1038/S41560-021-00881-Y;SUBJMETA.

[18] Y yu Yao, T. Wang, L guang Wu, H li Chen, PES mixed-matrix membranes incorporating ZIF-8@MXene nanocomposite for the efficient dye/salt separation, Desalination 543 (2022) 116116, https://doi.org/10.1016/J.DESAL.2022.116116.

[19] S. Yang, R. Tang, Y. Dai, T. Wang, Z. Zeng, L. Zhang, Fabrication of cellulose acetate membrane with advanced ultrafiltration performances and antibacterial properties by blending with HKUST-1@LCNFs, Sep. Purif. Technol. 279 (2021) 119524, https://doi.org/10.1016/J.SEPPUR.2021.119524.

[20] G. Liu, L. Li, X. Huang, S. Zheng, X. Xu, Z. Liu, Adsorption and removal of organophosphorus pesticides from environmental water and soil samples by using magnetic multi-walled carbon nanotubes @ organic framework ZIF-8, J. Mater. Sci. 53 (2018) 10772–10783, https://doi.org/10.1007/S10853-018-2352-Y/METRICS.

[21] Y. Wei, Y. Zhang, X. Gao, Y. Yuan, B. Su, C. Gao, Declining flux and narrowing nanochannels under wrinkles of compacted graphene oxide nanofiltration membranes, Carbon N Y 108 (2016) 568–575, https://doi.org/10.1016/J.CARBON.2016.07.056.

[22] V. Vatanpour, M.E. Pasaoglu, H. Barzegar, O.O. Teber, R. Kaya, , et al.M. Bastug, Cellulose acetate in fabrication of polymeric membranes: a review, Chemosphere 295 (2022) 133914, https://doi.org/10.1016/J.CHEMOSPHERE.2022.133914.

[23] P.D. Sutrisna, R.P. Hadi, J. Siswanto, G.J. Prabowo, The co2/ch4 separation potential of zif-8/polysulfone mixed matrix membranes for biogas upgradation process, Int. J. Renew. Energy Dev. 10 (2020) 213–219, https://doi.org/10.14710/ijred.2021.33118.

[24] P.D. Sutrisna, C. Wijaya, C. Robby, J. Liliani, ZIF-8/Cellulose acetate based mixed matrix membranes (MMMs) synthesis and characterization, Adv. Sci. Technol. 104 (2021) 57–64, https://doi.org/10.4028/www.scientific.net/AST.104.57.

[25] A. Nqombolo, T.A. Makhetha, R.M. Moutloali, P.N. Nomngongo, Flux and Fouling Behavior of Graphene Oxide-Polyphenylsulfone Ultrafiltration Membranes Incorporating ZIF-67/ZIF-8 Fillers, 15, 2025, p. 289, https://doi.org/10.3390/MEMBRANES15100289.

[26] A. Fatima, H.M. Saif, F.X. Nascimento, S. Pawlowski, J.G. Crespo, Selective lithium recovery using bacterial cellulose acetate membranes: toward green recycling of spent Li-ion batteries, J. Membr. Sci. (2025) 124776, https://doi.org/10.1016/J.MEMSCI.2025.124776.

[27] N.B.A. Prasetya, M.R. Putri, Gunawan Ngadiwiyana, Polyeugenol-gum arabic/graphene oxide composite coating for high performance anticorrosion material, Case Stud. Chem. Environ. Eng. 9 (2024) 100658, https://doi.org/10.1016/J.CSCEE.2024.100658.

[28] S.P. Dhongade, S.T. Malkapuram, S.H. Sonawane, High-performance graphene oxide–incorporated cellulose acetate membranes for efficient dye wastewater treatment, ChemistrySelect (2025), https://doi.org/10.1002/slct.202501810.

[29] Madih K, El-Shazly AH, Elkady MF, Aziz AN, Youssef ME, Khalifa RE, 26 (2022) 101435. https://doi.org/10.1016/J.JSCS.2022.101435.

[30] V. Vatanpour, A. Yuksekdag, M. Ağtaş, M.C.-M.R. Mehrabi, E. Salehi, Zeolitic imidazolate framework (ZIF-8) modified cellulose acetate NF membranes for potential water treatment application, Carbohydr. Polym. (2023), https://doi.org/10.1016/j.carbpol.2022.120230.

[31] P. Pillai, S. Dharaskar, S. Sasikumar, M. Khalid, Zeolitic imidazolate framework-8 nanoparticle: a promising adsorbent for effective fluoride removal from aqueous solution, Appl. Water Sci. 9 (2019) 1–12, https://doi.org/10.1007/S13201-019-1030-9/FIGURES/13.

[32] S.T. Malkapuram, M.M. Seepana, S.H. Sonawane, S.K. Lakhera, E. Randviir, ZIF-8 decorated cellulose acetate mixed matrix membrane: an efficient approach for

textile effluent treatment, Chemosphere 349 (2024), https://doi.org/10.1016/j.chemosphere.2023.140836, 2024.
[33] H.Y. Kim, Y. Cho, S.W. Kang, Porous cellulose acetate membranes prepared by water pressure-assisted process for water-treatment, J. Ind. Eng. Chem. 78 (2019) 421–424, https://doi.org/10.1016/J.JIEC.2019.05.027.
[34] A. Rajeswari, E. Jackcina Stobel Christy, G. Ida Celine Mary, K. Jayaraj, A. Pius, Cellulose acetate based biopolymeric mixed matrix membranes with various nanoparticles for environmental remediation-A comparative study, J. Environ. Chem. Eng. 7 (2019) 103278, https://doi.org/10.1016/J.JECE.2019.103278.
[35] M. Ali, M. Aslam, A. Khan, M.A. Gilani, A.L. Khan, Mixed matrix membranes incorporated with sonication-assisted ZIF-8 nanofillers for hazardous wastewater treatment, Environ. Sci. Pollut. Control Ser. 26 (2019) 35913–35923, https://doi.org/10.1007/s11356-019-06698-3.
[36] N. Nasrollahi, L. Ghalamchi, V. Vatanpour, A. Khataee, M. Yousefpoor, Novel polymeric additives in the preparation and modification of polymeric membranes: a comprehensive review, J. Ind. Eng. Chem. 109 (2022) 100–124, https://doi.org/10.1016/j.jiec.2022.02.036.
[37] A. Abdel-Karim, M.E. El-Naggar, E.K. Radwan, I.M. Mohamed, M. Azaam, E. R. Kenawy, High-performance mixed-matrix membranes enabled by organically/inorganic modified montmorillonite for the treatment of hazardous textile wastewater, Chem. Eng. J. 405 (2021) 126964, https://doi.org/10.1016/J.CEJ.2020.126964.
[38] D. Zheng, H. Yang, F. Yu, B. Zhang, H. Cui, Effect of Graphene Oxide on the Crystallization of Calcium Carbonate by C3S Carbonation, 12, 2019, p. 2045, https://doi.org/10.3390/MA12132045.
[39] L.C. Condes, M.T. Webb, T.T.B. Le, W.J. Box, C.M. Doherty, A. Gali, Elucidating the molecular mechanisms by which porous polymer networks affect structure, aging propensity, and selectivity of microporous glassy polymer membranes using a multiscale approach, ACS Appl. Mater. Interfaces 16 (2024) 53843–53854, https://doi.org/10.1021/acsami.4c11472, 2024;16:53843–54.
[40] M. Benzaqui, R. Semino, N. Menguy, F. Carn, T. Kundu, J.-M. Guigner, et al., Toward an understanding of the microstructure and interfacial properties of PIMs/ZIF-8 mixed matrix membranes, ACS Appl. Mater. Interfaces 8 (2016) 27311–27321, https://doi.org/10.1021/acsami.6b08954.
[41] V. Durán-Egido, D. García-Giménez, J.C. Martínez-López, C.-G.J. Pérez-Vidal L, Metal–organic frameworks as fillers in porous organic polymer-based hybrid materials: innovations in composition, processing, and applications. https://doi.org/10.3390/polym17141941, 2025.
[42] S. Park, H.K. Jeong, Cross-linked Polyimide/ZIF-8 mixed-matrix membranes by in situ formation of ZIF-8: effect of cross-linking on their Propylene/Propane separation. https://doi.org/10.3390/membranes12100964, 2022.
[43] S. Wang, Z. Gao, X. Qi, C. Li, Y. Xie, X. Yang, Eco-friendly superhydrophobic MOF-doped with cellulose acetate foam for efficient oil-water separation, J. Environ. Chem. Eng. 10 (2022) 108521, https://doi.org/10.1016/J.JECE.2022.108521.
[44] W. Shi, C. Xu, J. Cai, S. Wu, Advancements in material selection and application research for mixed matrix membranes in water treatment, J. Environ. Chem. Eng. 11 (2023) 111292, https://doi.org/10.1016/j.jece.2023.111292.
[45] P.D. Sutrisna, R.P. Hadi, C. Wijaya, J. Liliani, C. Robby, Cellulose acetate-based mixed matrix membrane for methylene blue wastewater treatment. https://doi.org/10.1063/5.0112184, 2023.
[46] D. Ma, S.B. Peh, G. Han, S.B. Chen, Thin-film nanocomposite (TFN) membranes incorporated with super-hydrophilic metal–organic framework (MOF) UiO-66: toward enhancement of water flux and salt rejection, ACS Appl. Mater. Interfaces 9 (2017) 7523–7534, https://doi.org/10.1021/ACSAMI.6B14223.
[47] S.R. Mousavi, M. Asghari, N.M. Mahmoodi, Chitosan-wrapped multiwalled carbon nanotube as filler within PEBA thin film nanocomposite (TFN) membrane to improve dye removal, Carbohydr. Polym. 237 (2020) 116128, https://doi.org/10.1016/j.carbpol.2020.116128.
[48] B. Hastuti, S. Nur Afifah, B. Mulyani, E. Susilowati, Adsorption of methylene blue dyes using pectin membrane, J. Phys., Conf. Ser. 1503 (2020) 012031, https://doi.org/10.1088/1742-6596/1503/1/012031.
[49] S. Wu, W. Shi, L. Cui, C. Xu, Enhancing contaminant rejection efficiency with ZIF-8 molecular sieving in sustainable mixed matrix membranes, Chem. Eng. J. (2024), https://doi.org/10.1016/j.cej.2024.148954.
[50] A. Gawali, S. Gawali, S.S. Jampa, M.K. Sinha, J. Pandya, S. Shinde, Study on water and gas permeation characteristics with ZIF-8 mixed matrix membranes, AQUA - Water Infrastructure, Ecosystems and Society 72 (2023) 1097–1114, https://doi.org/10.2166/AQUA.2023.102, 2023;72:1097–1114.
[51] Y. Yahia, K.T. Rashid, M.A. Shehab, A.A. Abdul Razak, M.Y. Ghadhban, M. Al-Lami, Treating wastewater contaminated with congo red (CR) dye using an optimized polyethersulfone/propolis (bee glue) PES/PRS ultrafiltration membrane, RSC Adv. 15 (2025) 23174–23186, https://doi.org/10.1039/d5ra03565a.
[52] S.P. Dhongade, S.T. Malkapuram, S.H. Sonawane, S. Manickam, High-performance MIL-53(Fe)-incorporated cellulose acetate membranes for efficient dye and wastewater treatment, Talanta Open 12 (2025) 100517, https://doi.org/10.1016/j.talo.2025.100517.
[53] Y. Song, R. Zhang, B. Dong, Y. Liu, M. Zhang, X. Hu, One-step engineering of multifunctional ZIF-8/PES membrane for synergistic separation of selected proteins, dyes and antibiotics, Desalination (2025), https://doi.org/10.1016/j.desal.2025.119377.